Retinal Vessel Caliber Measurement Bias in Fundus Images in the Presence of the Central Light Reflex

Pappelis, Konstantinos; Jansonius, Nomdo M.

Published in:
Translational Vision Science and Technology

DOI:
10.1167/tvst.12.7.16

Document Version
Publisher's PDF, also known as Version of record

Publication date:
2023

tvst

Retina

Retinal Vessel Caliber Measurement Bias in Fundus Images in the Presence of the Central Light Reflex

Konstantinos Pappelis[1,2] **and Nomdo M. Jansonius**[1,2]

[1] Department of Ophthalmology, University of Groningen, University Medical Center Groningen, Groningen, the Netherlands
[2] Graduate School of Medical Sciences, Research School of Behavioural and Cognitive Neurosciences, University of Groningen, Groningen, the Netherlands

Correspondence: K. Pappelis, Department of Ophthalmology, University Medical Center Groningen, PO Box 30.001, 9700 RB, Groningen, the Netherlands.
e-mail: k.pappelis@rug.nl

Received: January 17, 2023
Accepted: June 16, 2023
Published: July 14, 2023

Keywords: fundus imaging; scanning laser ophthalmoscope; retinal vessel caliber; central light reflex; hypertension

Citation: Pappelis K, Jansonius NM. Retinal vessel caliber measurement bias in fundus images in the presence of the central light reflex. Transl Vis Sci Technol. 2023;12(7):16, https://doi.org/10.1167/tvst.12.7.16

Purpose: To investigate the agreement between a fundus camera and a scanning laser ophthalmoscope in retinal vessel caliber measurements and to identify whether the presence of the central light reflex (CLR) explains potential discrepancies.

Methods: For this cross-sectional study, we obtained fundus camera and scanning laser ophthalmoscope images from 85 eyes of 85 healthy individuals (aged 50–65 years) with different blood pressure status. We measured the central retinal artery equivalent (CRAE) and central retinal artery vein equivalent (CRVE) with the Knudtson–Parr–Hubbard algorithm and assessed the CLR using a semiautomatic grading method. We used Bland–Altman plots, 95% limits of agreement, and the two-way mixed effects intraclass correlation coefficient for consistency [ICC(3,1)] to describe interdevice agreement. We used multivariable regression to identify factors associated with differences in between-device measurements.

Results: The between-device difference in CRAE (9.5 μm; 95% confidence interval, 8.0–11.1 μm) was larger than the between-device difference in CRVE (2.9 μm; 95% confidence interval, 1.3–4.5 μm), with the fundus camera yielding higher measurements (both $P < 0.001$). The 95% fundus camera–scanning laser ophthalmoscope limits of agreement were −4.8 to 23.9 μm for CRAE and −12.0 to 17.8 μm for CRVE. The corresponding ICCs(3,1) were 0.89 (95% confidence interval, 0.83–0.92) and 0.91 (95% confidence interval, 0.86–0.94). The between-device CRAE difference was positively associated with the presence of a CLR ($P = 0.002$).

Conclusions: Fundus cameras and scanning laser ophthalmoscopes yield correlated but not interchangeable caliber measurements. The CLR induces bias in arteriolar caliber in fundus camera images, compared with scanning laser ophthalmoscope images.

Translational Relevance: Refined measurements could yield better estimates of the association between retinal vessel caliber and ophthalmic or systemic disease.

Introduction

The retinal blood vessels have long been known to be implicated in major ophthalmic pathologies, such as glaucoma and age-related macular degeneration, as well as in diseases with ocular involvement, namely, diabetes and arterial hypertension.[1–4] Some of their properties, such as retinal vessel caliber, have also been suggested as promising biomarkers in the evaluation of various nonophthalmic pathologies, including atherosclerosis, coronary heart disease, and neurological diseases.[5–8] However, the assessment of retinal vessels is not entirely standardized and may be influenced by technical factors and different modalities, thus compromising potential applications in the clinical setting.

Recent advances in optical coherence tomography angiography have enabled the detailed, noninvasive visualization of downstream microcirculation to the capillary level, but the evaluation of the larger retinal vessels is still based predominantly on fundus imaging.[9–12] Retinal vessel caliber is often assessed qualitatively in the routine clinical evaluation of fundus

images.[13] However, several clinical and epidemiological studies have adopted a quantitative approach to retinal vessel caliber assessment, predicting the diameters of the central retinal vessels from the diameters of their visible daughter branches in the en face images.[14–17]

Retinal vessel caliber quantification is performed by various semiautomatic image analysis software programs that have been shown to not yield interchangeable measurements.[18–20] Nevertheless, even when the same image processing algorithms are used, vessel tracking could still be influenced by the choice of imaging modality.[21,22] Indeed, the numerous devices used for fundus imaging differ in terms of optical principles, properties of the light source, scattering, image acquisition, and image processing, among other aspects.[23,24] These factors could affect the vessel intensity profiles and, consequently, the detection of vessel edges. Another factor that could significantly affect profile-based edge detection is the presence of the central light reflex (CLR), that is, the hyper-reflective region running along the center of the blood column. The CLR appears mostly in arterioles, likely owing to the thickening and hardening of their walls, and is exacerbated in arterial hypertension, leading to phenotypes known as copper and silver wiring.[25] Biased estimates of retinal vessel caliber owing to the CLR could have an effect on the interpretation of clinical and epidemiological findings.

Therefore, the aim of this study was to investigate the agreement of retinal vessel caliber measurements between a color fundus camera and a scanning laser ophthalmoscope and to identify whether the presence of the CLR explains potential discrepancies. For this purpose, we collected high-resolution images of the retinal vasculature from ophthalmologically healthy individuals with different blood pressure (BP) statuses, we quantified the retinal vessel caliber with standard image processing methods, and we assessed the CLR using objective grading.

Methods

Study Design and Population

This is a cross-sectional study. We prospectively invited subjects between 50 and 65 years of age from the Lifelines Biobank, an ongoing cohort study in the northern Netherlands (n = 167,000). Selection was a priori based on BP profile, placing particular emphasis on including subjects consistently belonging to the tails of the BP distribution during their follow-up. The exact criteria, rationale, and power specifications of the recruitment process have been described extensively in our recent studies on the same population.[26,27] In short, the subjects included were required to fall into one of four predefined groups: low BP, normal BP, treated high BP, and untreated high BP. Subjects in the low BP group were invited based on documented recordings of systolic BP (SBP) and diastolic BP (DBP) that were below the respective 10th percentile of the population on two or more separate occasions. Subjects in the untreated high BP group were invited based on such recordings above the 90th percentile of the population. Subjects in the normal BP group were required to have no record of antihypertensive treatment, as well as both SBP and DBP within 1 standard deviation from the mean of the age-matched population. Finally, subjects in the treated high BP group were invited based on documented uninterrupted use of antihypertensive treatment for at least 1 year.

We obtained a medical history and screened all of the subjects who responded to our invitation. Regarding the ophthalmic screening, the inclusion criteria were best-corrected visual acuity of no less than 0.8 (20/25), spherical refractive error within –3 and +3 diopters, cylinder no more than 2 diopters, intraocular pressure no more than 21 mm Hg (noncontact tonometer Tonoref II; Nidek, Aichi, Japan), no reproducibly abnormal visual field test locations (Frequency Doubling Technology [C20-1 screening mode]; Carl Zeiss Meditec, Jena, Germany), no ophthalmic pathology or history of previous ophthalmic surgery, and no family history of glaucoma. Regarding general medical history, the exclusion criteria were: established diagnosis of diabetes, cardiovascular disease (except for arterial hypertension), hematologic disease, or lung disease.

All participants provided written informed consent. The ethics board of the University Medical Center Groningen approved the study protocol (#NL61508.042.17). The study followed the tenets of the Declaration of Helsinki.

Fundus Imaging

The imaging session was performed in the evening (between 5:00 PM and 6:30 PM) for all subjects. After screening, we applied 0.5% tropicamide eye drops and the participants rested in a dimly lit, quiet room for 20 minutes. Subsequently, we obtained brachial artery BP readings, in sitting position, with an automatic monitor (Omron M6 Comfort, Omron Healthcare, Kyoto, Japan). We recorded the average of two measurements unless there was a discrepancy of at least 10 mm Hg in SBP or 5 mm Hg in DBP, in which case we recorded the average of three measurements.

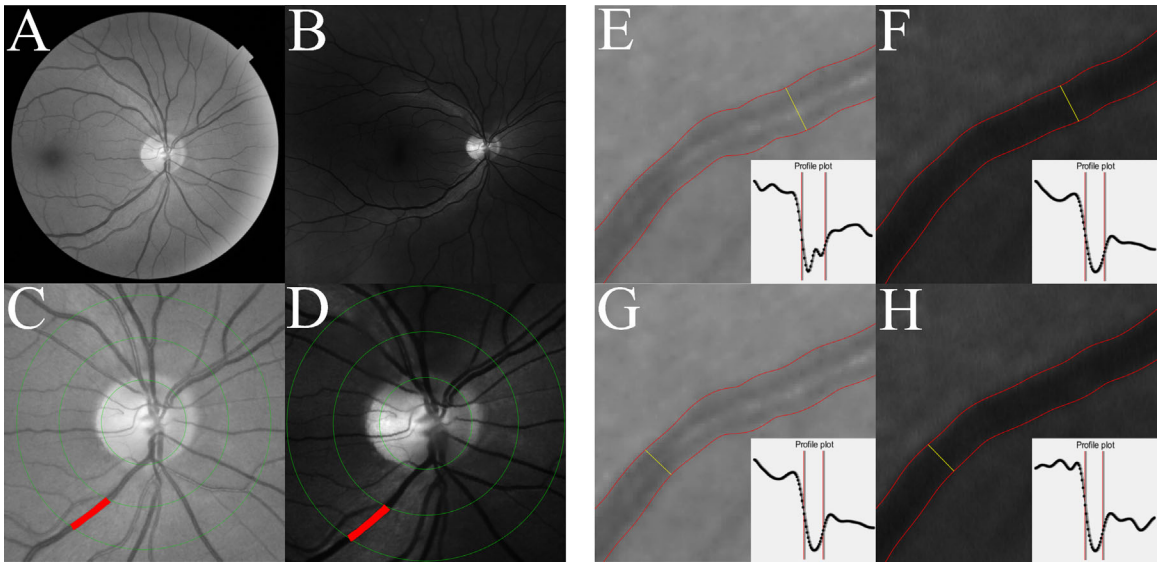

Figure 1. (**A**) Grayscale equivalent of the disc-centered 45° fundus image obtained with the TRC-NW400. (**B**) Grayscale equivalent of the ResMax image obtained with the 532-nm (*green*) laser of the Optomap 200Tx. (**C**, **D**) Disc-centered ring (inner and outer diameters equal to 2 and 3 optic disc diameters, respectively), within which the vessel diameter measurements were obtained for each imaging modality. The venule with the largest diameter in this region is marked in *red*. (**E**, **F**) Example of a delineated arteriole depicted with both modalities and the intensity profile plot at one of its cross-sections (marked in *yellow*). Edges appear further away in the image obtained by the TRC-NW400 (139 µm) compared with the Optomap 200Tx (110 µm), owing to the presence of the central light reflex in the former. (**G**, **H**) The same arteriole and the intensity profile plot at a different location, in absence of the central light reflex. Vessel diameter at this location is similar between the two devices (105 and 102 µm, respectively).

We obtained images from the eye that fulfilled the inclusion criteria, or from a random eye, if both did. We used a color fundus camera (TRC-NW400; Topcon Corporation, Tokyo, Japan) and a scanning laser ophthalmoscope (Optomap 200Tx; Optos PLC, Dunfermline, UK) in random order. Two 45° fundus images centered at the optic disc were obtained with the fundus camera, and two 60° (ResMax) images were obtained with the scanning laser ophthalmoscope, with the laser gain adjusted at moderately pigmented iris. The scanning laser ophthalmoscope simultaneously acquires two images, one at a wavelength of 532 nm (green) and the other at a wavelength of 633 nm (red). The retinal vasculature attains better contrast at the green wavelength, so we used those images for subsequent analysis.[28,29] All images were stored in an uncompressed format (.tiff).

For a participant to be included in the analysis, we required all four images (two images per device) to be artifact free and of high quality. Image quality was judged subjectively, following the grading criteria proposed by Laurik-Feuerstein et al.[30] In short, images were assessed for focus (sharp depiction of smaller order vessels and minor retinal alterations), illumination (absence of washed-out or dark areas interfering with grading), image field (proper centration allowing for grading of the region of interest), and absence of artifacts (camera reflexes, dust spots or fingerprints, eyelash images, or arc defects).

Vessel Segmentation

Analysis was performed with freely available, semiautomatic software (Automated Retinal Image Analyzer, Peter Bankhead), which was developed based on fundus images.[31] The software uses grayscale equivalents of the fundus images, generated from the green channel information (Figs. 1A–1B). Before segmentation, wavelet thresholding was applied to enhance vessel contrast. All images were segmented using the same preset threshold settings, smoothing scales, and wavelet levels. Vessel centerlines were subsequently generated following morphological thinning and spline fitting.

The measurement region was the standard disc-centered ring with inner and outer diameters equal to 2 and 3 optic disc diameters, respectively (Figs. 1C–1D).[15] The maximal distance d between two points at the border of the optic disc was marked by an experienced grader (K.P.), and a circle of diameter d was placed around the optic disc automatically. Because the shape of the optic disc can deviate from this circle and the area of the optic disc determines the exact location of the caliber measurements obtained, we also performed structural optical coherence

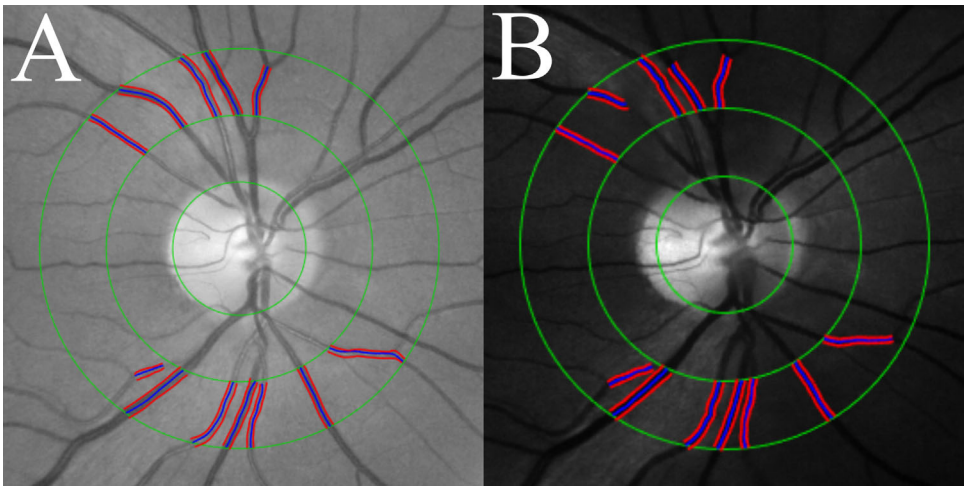

Figure 2. Cropped down fundus image (**A**) and scanning laser ophthalmoscope image (**B**) displaying the six largest arterioles and six largest venules within the measurement region. Vessel edges are marked in *red* and vessel centerlines are marked in *blue*. The calibers of these branches are iteratively used for the calculation of the central retinal artery and central retinal vein equivalents.

tomography imaging of the optic nerve head (Canon HS100 SD-OCT; Canon, Inc., Tokyo Japan) to obtain better estimates of its area. The optical coherence tomography apparatus automatically locates the borders of the optic disc at the opening of Bruch's membrane, following a circular scanning pattern.

Vessel edges were traced automatically within the region of interest. The software detects the edges in the direction perpendicular to the vessel centerlines. Edge detection is based on Gaussian-smoothed intensity profiles (Figs. 1E–1H), and the locations where the intensity gradient is maximal (i.e., zero-crossings of the second derivative) are used to define the vessel borders. All images were screened for obvious segmentation errors and were manually adjusted by an experienced observer (K.P.), when deemed necessary.

Vessel Diameter Measurement

The average diameter of each vessel within the region of interest was recorded in pixels. Pixels were transformed to units of length (μm) based on manufacturer specifications and Gullstrand's schematic eye, that is, assuming a distance of 17 mm between the secondary nodal point and the retina and not accounting for variations in corneal curvature or axial length.

We used the standard Knudtson–Parr–Hubbard algorithm, whose intragrader and intergrader reliability have been established previously as excellent.[15] In short, the six largest arterioles and six largest venules within the region of interest were identified and selected for analysis (Fig. 2). Subsequently, the largest and smallest arteriole were paired and merged into one single value (representing the hypothetical width of a parent trunk) using the formula provided below:

$$D_{parent} = 0.88\sqrt{D_{large}^2 + D_{small}^2},$$

where D denotes the arteriolar diameter and the factor 0.88 is a branching coefficient.

The same was applied to the second largest and second smallest arterioles, followed by the third largest and third smallest arterioles. Of the resulting three new values, the largest and smallest were merged again (using the same formula) and their output was finally merged with the previously unpaired value, yielding a singular value. The same procedure was repeated for the venules, but with a branching coefficient of 0.95.

These back-calculated singular values are known as the central retinal artery equivalent (CRAE) and central retinal vein equivalent (CRVE), and they represent the predicted calibers of the central retinal artery and vein, respectively. We also calculated their ratio (CRAE/CRVE), known as the arteriovenous ratio (AVR), which is often used to account for interindividual variability in vessel size and for errors in caliber measurements introduced owing to image magnification.[32] For each device, we recorded the average CRAE, CRVE, and AVR of the two images obtained.

CLR Quantification

We used the grayscale equivalents of the color fundus images to quantify the CLR because it was much more prominent in those images than in the scanning laser ophthalmoscope images. It is likely

that this is due to the color fundus images used containing intensity information from the red oxygen-sensitive wavelengths, resulting in increased contrast between the vessel walls and the blood column.[33] Additionally, according to the confocal principle, the laser ophthalmoscope would theoretically prevent any scattering occurring in more superficial layers. As shown in Figures 1E–1H, the locations where the CLR is present are characterized by an elevation in the corresponding vessel pixel intensity profile.

We quantified the CLR inside the same six arterioles used in the vessel diameter measurements and the same region of interest. Specifically, the CLR was classified as present in a vessel segment if at least 50% of its measured cross-sections displayed an elevation in their intensity profile. Vessel cross-sections were equidistant and each edge pixel belonged to exactly one cross-section. The CLR was classified as absent in all other cases. Based on the number of vessel segments with CLR, each fundus image was assigned a CLR score from 0 to 6.

Statistical Analyses

All normally distributed variables were described by the mean and standard deviation. Variables with a skewed distribution were described by the median and interquartile range. Comparisons between devices were performed with paired *t*-tests for normally distributed variables and with the Wilcoxon signed-rank test for variables with a skewed distribution. Pearson's r was used to establish correlations between normally distributed variables.

We used Bland–Altman plots, the coefficient of repeatability, and the two-way mixed effects intraclass correlation coefficient for consistency [ICC(3,1)] to describe intradevice repeatability for CRAE, CRVE, and AVR. We used Bland–Altman plots, 95% limits of agreement, and the ICC(3,1) to describe the inter-device agreement and interchangeability for the same variables. We used multivariable regression to examine the association between CLR and the between-device difference in arteriolar caliber, adjusting for potential confounders (disc area and spherical equivalent). The between-device difference in venular caliber was also included in the model to account for unexplained variance originating from image acquisition. Because of the well-known relationship between CLR and BP, a second multivariable model was also built, replacing the CLR with BP.

All analyses were performed using R (version 3.3.3; R Foundation for Statistical Computing, Vienna, Austria) and SPSS (version 28; IBM Corp., Armonk, NY). A *P* value of 0.05 or less was considered statistically significant.

Results

In total, 105 subjects satisfied the inclusion criteria. Owing to suboptimal quality or presence of artifacts in at least one image out of the four obtained, 20 subjects were excluded. Thus, 85 eyes from 85 patients were ultimately included in the analysis. The characteristics of the study sample are displayed in Table 1. The CLR was present in at least one vessel segment in 78.8% of the subjects.

Table 2 shows the CRAE, CRVE, and AVR, as measured by the fundus camera and scanning laser ophthalmoscope. The fundus camera yielded significantly larger values for all three variables. The between-

Table 1. Characteristics of the Study Population

Age, Years	56.0 (52.5 to 60.5)
Sex, % female	58.8
SBP, mm Hg	126 (113 to 147)
DBP, mm Hg	81 (69 to 90)
BMI, kg/m^2	24.8 (22.1 to 28.0)
IOP, mm Hg	13.8 ± 3.1
SEQ, D	0.00 (–0.94 to +0.94)
Disc area, mm^2	1.95 (1.70 to 2.30)
CLR score, % per score	0: 21.2
	1: 25.9
	2: 29.4
	3: 14.1
	4: 4.7
	5: 4.7
	6: 0.0

BMI, body mass index; CLR, central light reflex; DBP, diastolic blood pressure; IOP, intraocular pressure; SBP, systolic blood pressure; SEQ, spherical equivalent.

Values are median (interquartile range) or mean ± standard deviation unless otherwise indicated.

Table 2. Vessel Diameter Measurements

	FC	SLO	*P* Value
CRAE, µm	169.3 ± 15.2	159.7 ± 15.4	$\mathbf{7.2 \cdot 10^{-20}}$
CRVE, µm	240.9 ± 17.4	238.0 ± 18.0	$\mathbf{7.9 \cdot 10^{-4}}$
AVR	0.704 ± 0.056	0.672 ± 0.057	$\mathbf{2.3 \cdot 10^{-19}}$

AVR, arteriovenous ratio; CRAE, central retinal artery equivalent; CRVE, central retinal vein equivalent; FC, fundus camera; SLO, scanning laser ophthalmoscope.

Values are mean ± standard deviation. Boldface entries indicate statistical significance.

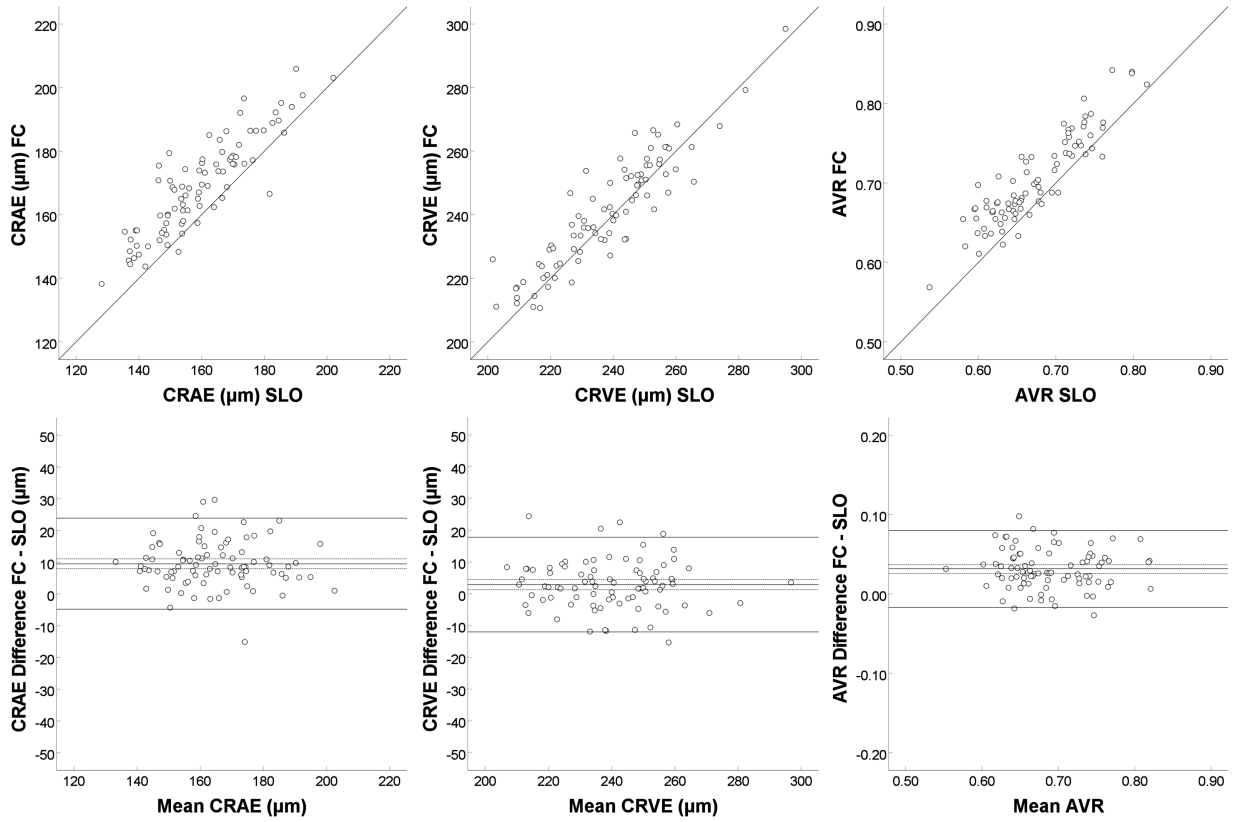

Figure 3. (*Top*) Absolute agreement between devices plotted for the central retinal artery equivalent (CRAE), the central retinal vein equivalent (CRVE), and the arteriovenous ratio (AVR). The $y = x$ line depicted is the line of absolute agreement. The majority of data points for all three metrics lie above the $y = x$ line, indicating that the TRC-NW400 yields larger diameter measurements than the Optomap 200Tx (*top left and middle*) and that this difference is larger in the arterioles than in the venules (*top right*). (*Bottom*) Bland–Altman plots showing the mean difference (dashed lines are 95% confidence intervals) of the measurements yielded by the two modalities and the bounds between which this difference is expected to be found 95% of the time. Differences between devices are not associated with mean values of devices, and the difference is larger in arterioles than in venules.

device difference in CRAE (9.5 µm; 95% confidence interval, 8.0–11.1 µm) was larger than the between-device difference in CRVE (2.9 µm; 95% confidence interval, 1.3–4.5 µm). Scatterplots for absolute agreement and Bland–Altman plots are presented in Figure 3. As shown in these plots, the magnitude of the observed between-device difference (bias) did not depend on the magnitude of the vessel caliber, averaged over both devices ($P_{CRAE} = 0.80$; $P_{CRVE} = 0.49$; $P_{AVR} = 0.67$), that is, the difference is a fixed offset rather than a factor.

Table 3 displays the between-device 95% limits of agreement and the between-device ICC for consistency, as well as the coefficient of repeatability and ICC for agreement within each device.

The left side of Figure 4 depicts the univariable association of the difference between the arteriolar measurements yielded by the two modalities and the CLR score. The difference increased significantly with increasing CLR (1.7 µm per unit change in CLR; $P = 0.004$). The right side of Figure 4 depicts the univariable association of the difference between arteriolar measurements and the difference between venular measurements. The differences were significantly associated ($P = 1.5 \cdot 10^{-8}$). Table 4 (Model A) displays the multivariable regression analysis with the difference between the arteriolar measurements as the dependent variable and the CLR score as the independent variable. When the CLR score is replaced in the model by SBP and DBP, higher SBP and lower DBP are associated with an increase in observed between-device CRAE difference (Table 4, Model B).

Discussion

In this study, we reported on the extent of agreement between a color fundus camera and a scanning laser ophthalmoscope in quantifying retinal vessel caliber.

Table 3. Intradevice and Interdevice Agreement and Consistency Metrics

	CoR (95% CI) FC	CoR (95% CI) SLO	95% LoA (95% CI) FC - SLO
CRAE (µm)	10.0 (8.9 to 11.0)	9.8 (8.7 to 10.9)	Lower: –4.8 (–6.4 to –3.3) Upper: 23.9 (22.3 to 25.5)
CRVE (µm)	11.6 (10.4 to 12.9)	11.9 (10.6 to 13.2)	Lower: –12.0 (–13.6 to –10.4) Upper: 17.8 (16.1 to 19.4)
AVR	0.044 (0.039 to 0.049)	0.041 (0.037 to 0.046)	Lower: –0.017 (–0.022 to –0.011) Upper:0.080 (0.075 to 0.085)
	ICC (95% CI) FC	ICC (95% CI) SLO	ICC (95% CI) between-device
CRAE	0.945 (0.917 to 0.964)	0.948 (0.922 to 0.966)	0.885 (0.828 to 0.923)
CRVE	0.944 (0.915 to 0.963)	0.945 (0.917 to 0.964)	0.908 (0.862 to 0.939)
AVR	0.923 (0.884 to 0.949)	0.935 (0.901 to 0.957)	0.905 (0.857 to 0.937)

AVR, arteriovenous ratio; CI, confidence interval; CoR, coefficient of repeatability; CRAE, central retinal artery equivalent; CRVE, central retinal vein equivalent; FC, fundus camera; ICC, intraclass correlation coefficient; LoA, limits of agreement; SLO, scanning laser ophthalmoscope.

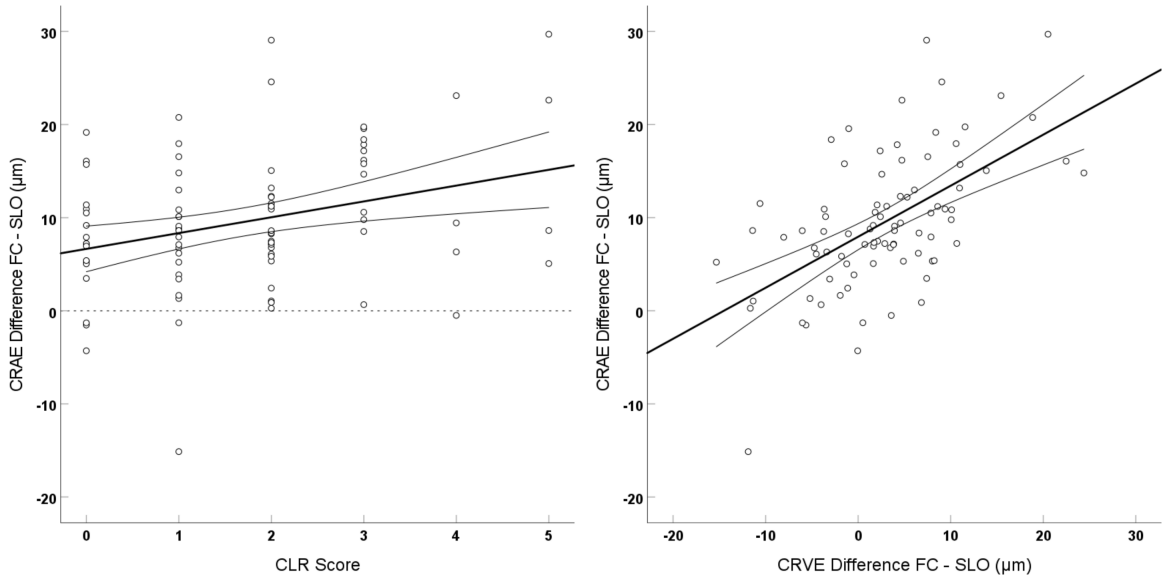

Figure 4. (*Left*) Difference between the arteriolar measurements yielded by the two modalities as a function of the central light reflex (CLR) grade (quantified from the TRC-NW400 images). The CLR grade ranges from 0 to 6 and depicts the number of measured vessels in which the light reflex appears in ≥50% of the cross-sections that are assessed along each vessel segment between the measurement circles. Difference increases with increasing presence of the CLR. The regression line is depicted with 95% confidence intervals of the slope. (*Right*) Difference between arteriolar measurements depicted as a function of the difference between venular measurements. Arteriolar difference increases with increasing venular difference. The regression line is depicted with 95% confidence intervals of the slope.

Table 4. Factors Associated With Observed Between-Device CRAE Difference: Multivariable Analysis

	CRAE Difference (FC - SLO; µm), Model A	
	Beta (95% CI)	*P* Value
CLR score	1.6 (0.6 to 2.6)	**.002**
CRVE difference (FC - SLO; µm)	0.5 (0.4 to 0.7)	**$1.6 \cdot 10^{-8}$**
Disc area (mm^2)	0.6 (–2.1 to 3.3)	.66
SEQ (D)	0.0 (–0.9 to 0.8)	.92
	CRAE Difference (FC - SLO; µm), Model B	
	Beta (95% CI)	*P* Value
SBP (mm Hg)	0.1 (0.0 to 0.2)	**.028**
DBP (mm Hg)	–0.2 (–0.4 to 0.0)	**.027**
CRVE difference (FC – SLO; µm)	0.5 (0.4 to 0.7)	**$1.9 \cdot 10^{-8}$**
Disc area (mm^2)	0.4 (–2.4 to 3.1)	.79
SEQ (D)	0.1 (–0.8 to 1.0)	.77

CI, confidence interval; CRAE, central retinal artery equivalent; CRVE, central retinal vein equivalent; CLR, central light reflex; DBP, diastolic blood pressure; FC, fundus camera; SBP, systolic blood pressure; SEQ, spherical equivalent; SLO, scanning laser ophthalmoscope.

Boldface entries indicate statistical significance.

We showed that, despite high intraclass correlation, vascular calibers derived from color fundus photography are larger compared with scanning laser ophthalmoscope images. This offset is more pronounced in arteriolar than venular calibers. Greater observed between-device difference in arteriolar caliber was associated with the presence of a more prominent CLR.

The caliber magnitudes that we reported in this study are generally in agreement with those reported in population studies implementing the standard Knudtson–Parr–Hubbard algorithm taking into consideration age and BP-related differences.[4,34–36] The vast majority of studies use color fundus cameras to quantify retinal vessel caliber; however, a few studies have used scanning laser ophthalmoscopes.[28,37] Automated quantification and grading of the CLR inside blood vessels is a more challenging and less explored task, while subjective grading could significantly compromise reproducibility.[38,39] To tackle these problems, we proposed an objective, semiautomatic method by making use of the vessel profiles obtained for caliber estimation.

The difference between the fundus camera-derived and scanning laser ophthalmoscope-derived retinal vessel caliber values reported in our study was an offset rather than a factor, because it was found to be independent of the measured caliber. In addition, the difference was larger in arteries than in veins. Therefore, magnification effects are highly unlikely to be the underlying cause of this observation, which is also corroborated by the fact that the spherical equivalent was not significant in multivariable analysis. Edge location algorithms used for vessel delineation usually rely on the half-width at half-maximum principle or on zero-crossings of the second derivative of the intensity profile.[31] The CLR renders the intensity dip less pronounced, introducing bias to the estimated edge location, thus resulting in a seemingly thicker vessel. In addition to the effect of the CLR on the intensity profile, it has been shown that edge location is also biased when low-pass filtered and nonlinearly transformed.[40,41] However, in contrast with the CLR, this phenomenon is less likely to explain the observed difference between arteries and veins because of the use of green channel information, in which arteries and veins appear with similar contrast. The between-device mean difference observed in this study was equal or less than the within-device coefficients of repeatability that, from a clinical perspective, suggests that devices are sufficiently interchangeable. Nevertheless, color fundus images are likely to be more informative for assessing the CLR, whereas vessel diameter measurements derived from scanning laser ophthalmoscope images are less affected by the confounding effect of the CLR. From an epidemiological perspective, our results suggest that the effect of cardiovascular disease on retinal vessel caliber is likely to be underestimated, because the CLR makes arteriolar calibers appear wider in color fundus images. Indeed, models A and B in Table 4 show that, owing to the CLR, patients with higher pulse pressure (usually a sign of pronounced

atherosclerosis and arteriosclerosis) are more likely to have higher retinal vessel caliber measurements in color fundus photographs. In all cases, it is important to introduce a standardized, objective protocol in retinal vessel caliber estimations.[32,42,43]

The main strengths of our study are the implementation of objective CLR quantification, as well as the fact that we were able to assess differences in vessel diameters in a wide range of BPs, from hypotensive individuals to treated or untreated hypertensives. One limitation of our study is the fact that vascular caliber was only quantified using one vessel processing software, but there may be disparities between different algorithms.[18–20] To date, there have been no studies investigating the performance of any vessel processing software in the presence of the CLR, and it is likely that some algorithms may be less affected than others. However, since edge detection is usually based on half-width at half-maximum or inflection principles, we hypothesize that this effect will be present on most occasions. Additional studies are needed to confirm this speculation. In addition, our population was predominantly Caucasian; hence, our results cannot be generalized safely to other ethnicities, especially owing to the documented effect of pigmentation on fundus contrast.[44] Finally, only the vessel lumen (blood column) is visible with conventional imaging techniques, which does not allow for assessment of the vessel wall. Adaptive optics have been used to visualize the vessel wall and quantify the wall-to-lumen ratio.[45,46]

In conclusion, we showed that the presence of a prominent CLR induces bias in retinal arteriolar caliber measurements in color fundus images, when compared with scanning laser ophthalmoscope images. Future population studies should use CLR-adjusted vessel diameters to obtain refined estimates of the relationship between retinal vessel caliber and ophthalmic or systemic diseases.

Acknowledgments

Financial Support: Stichting Oogfonds Nederland. The funding organization had no role in the design, conduct, analysis, or publication of this research.

Meeting Presentation: Association for Research in Vision and Ophthalmology (ARVO), Baltimore, May 3–7, 2020 (held online).

Disclosure: **K. Pappelis**, None; **N.M. Jansonius**, None

References

1. Mitchell P, Leung H, Wang JJ, et al. Retinal vessel diameter and open-angle glaucoma: the Blue Mountains Eye Study. *Ophthalmology*. 2005;112:245–250.
2. Jeganathan VSE, Kawasaki R, Wang JJ, et al. Retinal vascular caliber and age-related macular degeneration: the Singapore Malay Eye Study. *Am J Ophthalmol*. 2008;146:954–959.e1.
3. Klein R, Klein BEK, Moss SE, Wong TY. Retinal vessel caliber and microvascular and macrovascular disease in type 2 diabetes: XXI: the Wisconsin Epidemiologic Study of Diabetic Retinopathy. *Ophthalmology*. 2007;114:1884–1892.
4. Ikram MK, Witteman JCM, Vingerling JR, Breteler MMB, Hofman A, de Jong PTVM. Retinal vessel diameters and risk of hypertension: the Rotterdam Study. *Hypertension*. 2006;47:189–194.
5. Klein R, Sharrett AR, Klein BE, et al. Are retinal arteriolar abnormalities related to atherosclerosis?: The Atherosclerosis Risk in Communities Study. *Arterioscler Thromb Vasc Biol*. 2000;20:1644–1650.
6. McGeechan K, Liew G, Macaskill P, et al. Prediction of incident stroke events based on retinal vessel caliber: a systematic review and individual-participant meta-analysis. *Am J Epidemiol*. 2009;170:1323–1332.
7. Baker ML, Marino Larsen EK, Kuller LH, et al. Retinal microvascular signs, cognitive function, and dementia in older persons: the Cardiovascular Health Study. *Stroke*. 2007;38:2041–2047.
8. Guo S, Yin S, Tse G, Li G, Su L, Liu T. Association between caliber of retinal vessels and cardiovascular disease: a systematic review and meta-analysis. *Curr Atheroscler Rep*. 2020;22:16.
9. Jia Y, Tan O, Tokayer J, et al. Split-spectrum amplitude-decorrelation angiography with optical coherence tomography. *Opt Express*. 2012;20:4710–4725.
10. Pappelis K, Jansonius NM. Quantification and Repeatability of vessel density and flux as assessed by optical coherence tomography angiography. *Transl Vis Sci Technol*. 2019;8:3.
11. Pappelis K, Choritz L, Jansonius NM. Microcirculatory model predicts blood flow and autoregulation range in the human retina: in vivo investigation with laser speckle flowgraphy. *Am J Physiol Heart Circ Physiol*. 2020;319:H1253–H1273.
12. Al-Nosairy KO, Prabhakaran GT, Pappelis K, Thieme H, Hoffmann MB. Combined multimodal assessment of glaucomatous damage with

electroretinography and optical coherence tomography/angiography. *Transl Vis Sci Technol*. 2020;9:7.
13. Wong TY, Mitchell P. Hypertensive retinopathy. *N Engl J Med*. 2004;351:2310–2317.
14. Hubbard LD, Brothers RJ, King WN, et al. Methods for evaluation of retinal microvascular abnormalities associated with hypertension/sclerosis in the Atherosclerosis Risk in Communities Study. *Ophthalmology*. 1999;106:2269–2280.
15. Knudtson MD, Lee KE, Hubbard LD, Wong TY, Klein R, Klein BEK. Revised formulas for summarizing retinal vessel diameters. *Curr Eye Res*. 2003;27:143–149.
16. Wong TY, Klein R, Nieto FJ, et al. Retinal microvascular abnormalities and 10-year cardiovascular mortality: a population-based case-control study. *Ophthalmology*. 2003;110:933–940.
17. Amerasinghe N, Aung T, Cheung N, et al. Evidence of retinal vascular narrowing in glaucomatous eyes in an Asian population. *Invest Ophthalmol Vis Sci*. 2008;49:5397–5402.
18. French C, Heitmar R. Comparison of static retinal vessel caliber measurements by different commercially available platforms. *Optom Vis Sci*. 2021;98:1104–1112.
19. Yip W, Tham YC, Hsu W, et al. Comparison of common retinal vessel caliber measurement software and a conversion algorithm. *Transl Vis Sci Technol*. 2016;5:11.
20. Mautuit T, Cunnac P, Cheung CY, et al. Concordance between SIVA, IVAN, and VAMPIRE software tools for semi-automated analysis of retinal vessel caliber. *Diagnostics (Basel)*. 2022;12:1317.
21. Mautuit T, Semecas R, Hogg S, et al. Comparing measurements of vascular diameter using adaptative optics imaging and conventional fundus imaging. *Diagnostics (Basel)*. 2022;12:705.
22. Heitmar R, Kalitzeos AA. Reliability of retinal vessel calibre measurements using a retinal oximeter. *BMC Ophthalmol*. 2015;15:184.
23. Terasaki H, Sonoda S, Tomita M, Sakamoto T. Recent advances and clinical application of color scanning laser ophthalmoscope. *J Clin Med Res*. 2021;10:718.
24. DeHoog E, Schwiegerling J. Fundus camera systems: a comparative analysis. *Appl Opt*. 2009;48:221–228.
25. Kaushik S, Tan AG, Mitchell P, Wang JJ. Prevalence and associations of enhanced retinal arteriolar light reflex. *Ophthalmology*. 2007;114:113–120.
26. Pappelis K, Jansonius NM. Retinal oxygen delivery and extraction in ophthalmologically healthy subjects with different blood pressure status. *Transl Vis Sci Technol*. 2022;11:9.
27. Pappelis K, Jansonius NM. U-shaped effect of blood pressure on structural OCT metrics and retinal perfusion in ophthalmologically healthy subjects. *Invest Ophthalmol Vis Sci*. 2021;62:5.
28. Blair NP, Wanek J, Felder AE, et al. Retinal oximetry and vessel diameter measurements with a commercially available scanning laser ophthalmoscope in diabetic retinopathy. *Invest Ophthalmol Vis Sci*. 2017;58:5556–5563.
29. Hoover AD, Kouznetsova V, Goldbaum M. Locating blood vessels in retinal images by piecewise threshold probing of a matched filter response. *Proc AMIA Symp*. 1998:931–935.
30. Laurik-Feuerstein KL, Sapahia R, Cabrera DeBuc D, Somfai GM. The assessment of fundus image quality labeling reliability among graders with different backgrounds. *PLoS One*. 2022;17:e0271156.
31. Bankhead P, Scholfield CN, McGeown JG, Curtis TM. Fast retinal vessel detection and measurement using wavelets and edge location refinement. *PLoS One*. 2012;7:e32435.
32. Heitmar R, Vonthein R. Clinically valid conclusions from retinal photographs need the best formulae. *Graefes Arch Clin Exp Ophthalmol*. 2021;259:811–813.
33. Ouyang Y, Shao Q, Scharf D, Joussen AM, Heussen FM. An easy method to differentiate retinal arteries from veins by spectral domain optical coherence tomography: retrospective, observational case series. *BMC Ophthalmol*. 2014;14:66.
34. Ikram MK, Kamran Ikram M, de Jong FJ, et al. Are retinal arteriolar or venular diameters associated with markers for cardiovascular disorders? The Rotterdam Study. *Invest Ophthalmol Vis Sci*. 2004;47:189–194.
35. Gepstein R, Rosman Y, Rechtman E, et al. Association of retinal microvascular caliber with blood pressure levels. *Blood Press*. 2012;21:191–196.
36. Kawasaki R, Cheung N, Wang JJ, et al. Retinal vessel diameters and risk of hypertension: the Multiethnic Study of Atherosclerosis. *J Hypertens*. 2009;27:2386–2393.
37. Garg G, Venkatesh P, Chawla R, Takkar B, Temkar S, Damodaran S. Normative data of retinal arteriolar and venular calibre measurements determined using confocal scanning laser ophthalmoscopy system - Importance and implications for study of cardiometabolic disorders. *Indian J Ophthalmol*. 2022;70:1657–1663.
38. Bhuiyan A, Cheung CY, Frost S, et al. Development and reliability of retinal arteriolar central light reflex quantification system: a new approach

for severity grading. *Invest Ophthalmol Vis Sci*. 2014;55:7975–7981.
39. Nguyen UTV, Bhuiyan A, Park LAF, et al. An automated method for retinal arteriovenous nicking quantification from color fundus images. *IEEE Trans Biomed Eng*. 2013;60:3194–3203.
40. Jansonius NM, Cervantes J, Reddikumar M, Cense B. Influence of coherence length, signal-to-noise ratio, log transform, and low-pass filtering on layer thickness assessment with OCT in the retina. *Biomed Opt Express*. 2016;7:4490–4500.
41. Jansonius NM, Stam L, de Jong T, Pijpker BA. Quantitative analysis of illusory movement: spatial filtering and line localization in the human visual system. *Perception*. 2014;43:1329–1340.
42. Heitmar R, Kalitzeos AA, Patel SR, Prabhu-Das D, Cubbidge RP. Comparison of subjective and objective methods to determine the retinal arteriovenous ratio using fundus photography. *J Optom*. 2015;8:252–257.
43. Liew G, Sharrett AR, Kronmal R, et al. Measurement of retinal vascular caliber: issues and alternatives to using the arteriole to venule ratio. *Invest Ophthalmol Vis Sci*. 2007;48:52–57.
44. Rochtchina E, Wang JJ, Taylor B, Wong TY, Mitchell P. Ethnic variability in retinal vessel caliber: a potential source of measurement error from ocular pigmentation? The Sydney Childhood Eye Study. *Invest Ophthalmol Vis Sci*. 2008;49:1362–1366.
45. Streese L, Brawand LY, Gugleta K, Maloca PM, Vilser W, Hanssen H. New frontiers in noninvasive analysis of retinal wall-to-lumen ratio by retinal vessel wall analysis. *Transl Vis Sci Technol*. 2020;9:7.
46. Hillard JG, Gast TJ, Chui TYP, Sapir D, Burns SA. Retinal arterioles in hypo-, normo-, and hypertensive subjects measured using adaptive optics. *Transl Vis Sci Technol*. 2016;5:16.